Effectiveness of beads for tracking small-scale molecular motor dynamics

Steven J. Lade*
Nonlinear Physics Centre, Research School of Physics and Engineering, The Australian National University, Canberra, ACT 0200, Australia

Erin M. Craig
Department of Neurobiology, Physiology and Behavior and Department of Mathematics, University of California, Davis, California 95616, USA

Heiner Linke
The Nanometer Structure Consortium (nmC@LU) and Division of Solid State Physics, Lund University, S-22100 Lund, Sweden
(Received 6 April 2011; published 5 August 2011)

Investigations into molecular motor dynamics are increasingly focused on small-scale features of the motor's motion. We define performance measures of a common type of single-molecule motility assay, the bead assay, for its ability to detect such features. Using numerical models, we explore the dependence of assay performance on a number of experimentally controllable parameters, including bead size, optical force, and the method of attaching the bead to the motor. We find that the best parameter choice depends on the objective of the experiments, and give a guide to parameter selection. Comparison of the models against experimental data from a recent bead assay of myosin V exemplifies how our methods can also be used to extract additional information from bead assays, particularly that related to small-scale features. By analyzing the experimental data we find evidence for previously undetected multiple waiting states of the bead-motor complex. Furthermore, from numerical simulations we find that equilibrium bead dynamics display features previously attributed to aborted motor steps, and that bead dynamics alone can produce multiple subphases during a step.

DOI: 10.1103/PhysRevE.84.021907 PACS number(s): 87.16.Nn, 87.10.Mn

I. INTRODUCTION

Molecular motors such as myosin V and kinesin are naturally occurring, nanoscale machines that transport cargo within eukaryotic cells [1]. Although significant progress has been made toward understanding their motion, for example, that both myosin V and kinesin walk "hand-over-hand" [2,3], many aspects remain unresolved. Questions remain over the stepping dynamics of kinesin [4,5], including claim and counterclaim over the existence of substeps 3 to 4 nm long [6–9]. For the myosin V motor, the existence and size of substeps [10,11], the presence of the so-called "telemark" state [12–15], and other aspects of its stepping dynamics [10,16–19] are all under investigation.

Many experiments aiming to resolve such questions use the "bead assay" [6,8,10,11], where an artificial bead is attached to the motor, manipulated by optical tweezers [20,21] and its position monitored as a substitute for that of the motor itself. Indeed, this technique was used by Svoboda *et al.* [22] in their seminal studies of kinesin steps. The very first observations of kinesin stepping were also made with a similar technique [23].

We consider two mechanisms that may affect a bead assay's ability to accurately infer properties of the motor. First, the bead is not fixed relative to the motor, since the attachment between bead and motor may deform and since the bead can rotate about the motor. These effects are magnified when the bead is much larger than the motor, which is usually the case [22,24]. Second, the bead (or a cargo) can affect the behavior of the motor itself, for example, its velocity and gait [25–28]. Here we focus on assays investigating small-scale motor dynamical features, which require small spatial and fast temporal resolutions.

Using three-dimensional numerical models of a bead and motor, we define and calculate measures of a bead assay's ability to detect such small-scale features, including bead noise, response time, and stepping time. To aid design and interpretation of future assays, we investigate the dependence of these performance measures on controllable experimental parameters. Parameters we consider include the way the bead is attached to the motor, the optical tweezer force, the size of the bead, and the presence of a substrate. The choice of parameters will change according to the experiment's objectives we find, and we give a guide to their selection.

We also compare the bead dynamics in the models against a recent myosin V bead assay [10] using their Kramers-Moyal coefficients, which are position-dependent, short-time, effective drift and diffusion coefficients [29]. We find in the experimental data evidence for multiple waiting states that had not previously been detected. Furthermore, forward excursions of the bead, which were previously interpreted as aborted motor steps, we find are also consistent with the normal behavior of the bead-motor complex at equilibrium. Finally, we find that the dynamics of the bead alone can produce fast and slow phases during a motor step, similar to experimentally observed phases that previously were ascribed to motor dynamics.

II. MODELS AND DATA

To investigate the bead's dynamics independently of the motor's, our first class of models assumes the point where

*Current address: Max Planck Institute for the Physics of Complex Systems, Nöthnitzer Str. 38, D-01187 Dresden, Germany.

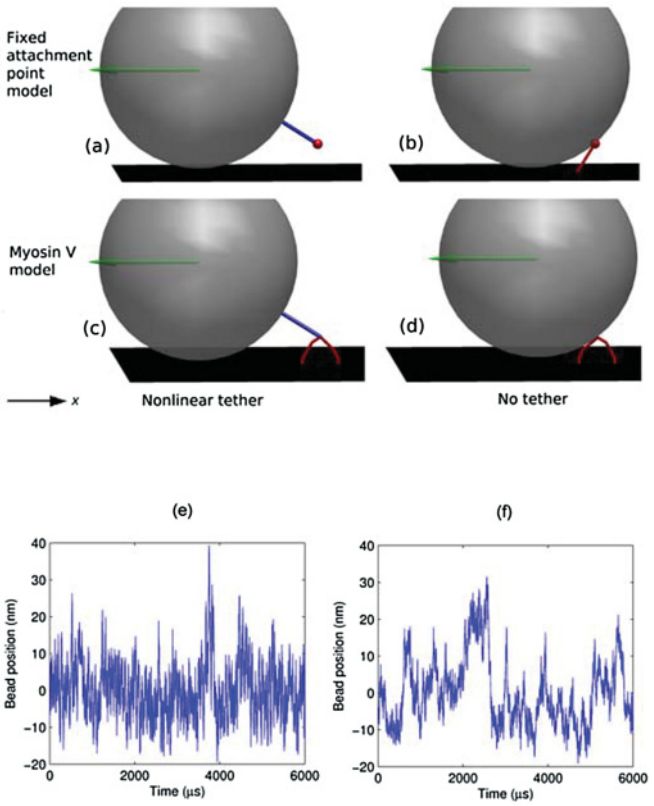

FIG. 1. (Color online) (a)–(d) Schematic summary of the models and bead attachments. In the myosin V model [(c) and (d)], the bead (large gray sphere) is attached to a biologically realistic mechanical model [30] of the myosin V molecular motor (red two-legged shape) with either a nonlinear tether [(a) and (c) blue rod connecting motor and bead] or no tether [(b) and (d)]. In the fixed-attachment-point model [(a) and (b)], the bead through its tether attaches to a point on the motor rigidly fixed in space (small red sphere). The fixed-attachment-point model (b) also includes steric interactions between the bead and a fixed trailing leg (red rod). In all models the motor will preferentially walk in the x direction, against the optical force (green arrow pointing left from center of bead), along an actin filament (not shown) attached to the substrate (black surface). "Position" in this article refers to displacement in the x direction, unless stated otherwise. (e) The output of each model is a time series of bead position, the properties of which are then analyzed. A sample time series is shown here. (f) A sample time series from the experimental data. A likely cause for the faster fluctuations in the model (e) compared to experiment (f) is our estimate of the bead's damping coefficient, as explained in the text.

the bead attaches to the motor is fixed [as in Figs. 1(a) and 1(b)]. A second class of models [sketched in Figs. 1(c) and 1(d)] investigates the effect of the bead on motor dynamics using extensions to a previous model of myosin V [30]. We vary parameters of these models, including the type of bead-motor connection and the presence of steric interactions, as summarized in Table I and described in more detail below. We take as their output time series of bead position [such as that in Fig. 1(e)]. We also compare these models' time series against a recent myosin V bead assay [10]. As described below, our parameters for both classes of models match this assay.

Both models incorporate Brownian forces acting on the bead or motor elements. As sketched in Fig. 1, both models also have an optical force, which we assume to be constant over a single step of the motor. The force acts on the center of mass of the bead and parallel to the motor track, and originates from the restoring force of the optical tweezers. As we will discuss, the optical force constrains the bead's motion. It can also serve as a load force in experiments.

A. Numerical fixed-attachment-point model of bead

This model simulates the dynamics of the bead alone. The Brownian and optical forces described above cause the bead to rotate in three-dimensional space about its attachment point to the motor, and its tether (if present, see below) to expand or contract. To reflect the structure of myosin V, we set the attachment point to a fixed location at 29 nm above the substrate [31]. The bead may also interact sterically (via "excluded volume") with a substrate, if present. In the no tether case, steric interactions with a fixed trailing neck domain are also included [as sketched in Fig. 1(d)]. No other aspects of the myosin V motor are explicitly modeled. See Ref. [31] for the mathematical formulation of the model.

We analytically projected the fixed-attachment-point model onto the x axis [31] to permit faster prediction of some bead properties. Analytical calculation of the drift coefficients involves assumption of the Markov property (that is, the projected system has no memory). Although the approximation is accurate (Fig. S3 of [31]), we verify all analytical predictions with direct numerical calculations.

B. Numerical model of bead attached to myosin V

We extend a previous coarse-grained, Brownian, mechanochemical model of myosin V [30] to include a large viscous bead. This model treats the neck domains as semielastic filaments with state-dependent attachment angles to the actin-binding heads, and assumes a flexible juncture between neck domains. This structure and its mechanical parameters were constrained by previous experimental results. Simulations were carried out using Brownian dynamics, in which the positional coordinates of the motor components were updated based on internal forces and external thermal noise forces. The results of the model have shown good agreement with experimental performance characteristics including stall force and processivity [30].

The model's dominant cycle is through three distinct mechanical states. There is a two-head bound, approximately symmetrical state that we refer to as the "pre-phosphate-release" (state I in Ref. [30]). Following phosphate release from the leading head, the motor is stressed into the so-called "telemark"' state (state II in Ref. [30]). The trailing head then unbinds and searches for the next binding site on the actin filament in the "diffusional search" state (state III in Ref. [30]). In experiments, the actin filament is usually fixed by attachment to a substrate.

To this model we added a bead, connected to the motor by either of the two attachments described below, and an optical force acting on the bead [31]. The bead interacts sterically with the motor and substrate. In the simulations required for

TABLE I. Model parameters varied to explore effects on bead assays.

	Line and marker colors and styles in Figs. 2(d) and 3–5				
Model parameters	Red dot-dashed line and crosses	Green line with cross-ticks and triangles	Dark blue dotted line and diamonds	Light blue dashed line and squares	Purple solid line and asterisks
Bead attachment[a]	NL	NL	NT	NT	NT
Substrate	No	Yes	No	No	Yes
Steric bead-motor interactions[b]	No	No	No	Yes	Yes
Bead diameter	0 to 500 nm				
Optical force	0 to 1.5 pN				

[a]NL and NT refer to beads attached by a nonlinear tether and no tether, respectively.
[b]For the fixed-attachment-point model. The myosin V model always models steric interactions between the motor and bead.

Fig. 2, the motor was initialized in state I (though we found no significant difference in the results when the motor was initialized in state II) and state transitions were suppressed. In the simulations required for Fig. 5, the model was initialized in state II, allowed to equilibrate, and then forced into state III.

We estimated damping coefficients for the bead (and other bodies) using Stokes' law. As will be shown in Figs. 2(a) and 2(b), this produced model drift and diffusion coefficients about a factor of 5 larger than the experimentally measured drift and diffusion coefficients. This difference could partially, but not completely [31], be caused by the increase in effective damping coefficient of a bead near a surface [21]. In the absence of a clear physical explanation for the full discrepancy, we chose neither to incorporate surface effect corrections nor to attempt to tune the diffusion coefficients into agreement, in both myosin V and fixed attachment point models.

This discrepancy in diffusion coefficients may lead to some quantitative changes in the properties calculated below. We have confirmed by simulation [31], however, that all key qualitative results are affected by neither the choice of bead damping coefficient, nor that the damping coefficient may depend on the bead's proximity to the substrate.

C. Bead attachments

There is much evidence for both myosins [32] and kinesin [6,22] that in bead assays the connection through the motor between the bead and motor track is nonlinear. A nonlinear connection also aids motor performance [26].

When connected to the end of kinesin's or myosin V's natural tether or "tail," this nonlinearity is due, in the normal region of the motor's operation, to entropic effects in the tail's uncoiling [32] leading to a nonlinear stiffness. In the nonlinear tether configuration [as sketched Figs. 1(a) and 1(c)] we model the bead as connected to the motor with a tether of the nonlinear elasticity found by Schilstra and Martin [26] for myosin V, based on experimental results combined with theoretical considerations. They found that a good model for the tether's restoring force when at length ϵ nm is $f(\epsilon) = 0.005\epsilon + (0.018\epsilon)^{10}$ pN.

A nonlinear stiffness between bead and motor may in principle also be achieved, as we will show, by affixing the bead directly (or with a short tether) to the motor and allowing the bead to rotate freely about this point. This is the "no tether" model [sketched in Figs. 1(b) and 1(d)].

D. Myosin V bead assay

We used time series of the x coordinate of bead position in the myosin V assay of Cappello *et al.* [10]. A section of one such time series is shown in Fig. 1(f). Their assay used a 200 nm bead. Except when being explicitly varied, we use the same bead size in our models. The time series available were at 2 mM ATP concentration and were already separated into steps and what we will refer to as "waiting periods," where the motor was not stepping and the bead distribution was approximately (statistically) stationary.

III. METHODS

We now outline the methods we used to analyze the model and experimental time series data.

A. Model characterization

The numerical and experimental time series $x(t)$ were characterized with the Kramers-Moyal coefficients [29]

$$D^{(n)}(x_0) = \lim_{\tau \to 0} \frac{1}{n!\tau} \langle [x(t+\tau) - x(t)]^n \, | x(t) = x_0 \rangle.$$

For $n = 1$ and 2 these are the drift and diffusion coefficients, respectively. Note these are local, or short-time quantities. "Diffusion coefficient" throughout this article refers to this definition, rather than a long-time mean-square displacement, unless otherwise noted. If the time series is nearly Markovian, then the drift and diffusion coefficients often fully characterize the process, including its equilibrium probability density; but if not, they still yield useful information about the process [33]. From an analytical model the drift and diffusion coefficients can be extracted directly [34], while from a numerical or experimental time series they can be approximated by stopping the limit at the sampling interval and replacing the conditional part of the expectation with a binning procedure. If the sampling interval is not small, biases can arise [35], but this was not the case for the bead here. The 0.3 nm (white, uncorrelated) experimental noise [36], which is small in comparison to the movement of the bead should add a constant offset of 0.1 $\text{nm}^2/\mu\text{s}$ to the estimated diffusion

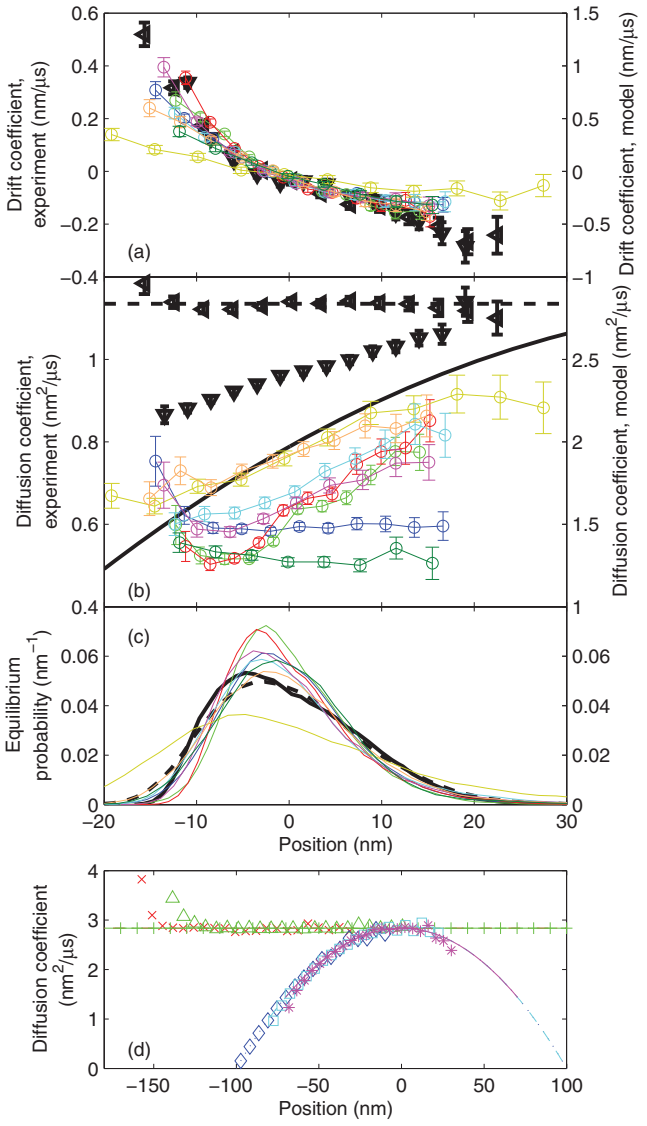

FIG. 2. (Color online) Characterization of bead motion in models and bead assay. (a) Drift, (b) diffusion, and (c) equilibrium probability distribution for the motion parallel to the motor track of the stationary sections of the experimental data of Cappello *et al*. [10] (colored thin lines, left axes) and our myosin V model (black, thick lines and markers, right axes) of Figs. 1(c) and 1(d). Results from the myosin V model are plotted for a bead connected by nonlinear tether [thick black left-pointing triangles, and thick dashed line in (c)] and no tether [thick black downward-pointing triangles, and thick solid line in (c)]. The position axis is with respect to the mean of each time series. Also plotted in (b) are the analytical results for the diffusion coefficients of beads attached to a fixed point with a nonlinear tether (thick dashed line) and no tether (thick solid line). (d) Diffusion coefficients for the motion parallel to the motor track in the fixed attachment point model. Results were calculated with the three-dimensional numerical model (markers) and its one-dimensional analytical simplification (lines). Line and marker colors and styles are as listed in Table I. The position axis is with respect to the bead attachment point.

coefficient, and not affect the estimated drift coefficient [37]. During the analysis we confirmed that the sets of increments $[x(t+\tau)-x(t)]_{x(t)=x_0}$ were normally distributed. The code used to calculate the drift and diffusion coefficients is provided in Ref. [31].

B. Response time prediction and estimation

By Onsager's mean regression hypothesis [38], the time for a phase variable of a system near equilibrium to return to equilibrium, its response time, is also the correlation time of that phase variable in equilibrium. For the numerical models, the bead's average correlation time in equilibrium t_{corr} was estimated through the Green-Kubo relation [38,39] $t_{\mathrm{corr}}\sigma_x^2 = D_\infty(\int x)$, where $\int x(t) \equiv \int_0^t [x(t') - \bar{x}]dt'$ and $\bar{x}$ and σ_x^2 are the mean and variance of $x(t)$, respectively. The *long-time* diffusion coefficient of the process $y(t)$, $D_\infty(y) = \lim_{t\to\infty} [\langle y(t)\rangle - y(0)]^2/2t$, was estimated by averaging over independent pairs at delay t of a single time series [40], to shorten computation time, then averaging over the delays at which the D_∞ estimates plateaued. For the analytical projection, the response (correlation) time could be predicted nonstochastically by the formula of Jung and Risken [41], but we found that due to the assumptions involved in the projection the correlation time predictions were not accurate. The projection captures the short time scales in the bead's motion through the drift and diffusion coefficients very well ([31], Fig. S3); however, the bead response time is limited by the longest time scales. These time scales involve, for example, motion of the bead transverse to the motor track changing the range of motion parallel to the track that steric interactions allow.

IV. CHARACTERIZATION OF MODELS AND MYOSIN V BEAD ASSAY

Our first goal is to investigate whether the experimental parameters and configuration, for example the type of bead attachment, can be inferred from position time series of the bead. This could be useful in characterizing assays where, for example, the chemistry of the bead attachment is not precisely known, or for verifying that the bead was attached as intended. Equilibrium probability distributions are one way to characterize these time series, but the (local) drift and diffusion coefficients or "Kramers-Moyal coefficients" [29], as introduced in Sec. III A, we will show reveal more information about the motion of the bead. The drift coefficient amounts to a position-dependent effective force, and is most useful for inferring potentials. The diffusion coefficient amounts to an effective temperature, and can be useful for inferring geometry [33,42].

Drift and diffusion coefficients, along with equilibrium probability distributions, are shown in Figs. 2(a)–2(c) for the waiting periods in the time series of Cappello *et al*. [10] and the numerical myosin V model. In the simulations, a substrate was included and an optical force of 0.83 pN was used in order to match the standard deviation of the experimental data; this is the only parameter that was tuned. The experimental time series used were the eight longest of the waiting periods available for analysis; all were at least 20 ms long.

Figure 2(c) shows that little distinction between the model configurations can be drawn on the basis of the probability distributions, for which (with one exception) the agreement

with experiment is excellent. The drift coefficients in Fig. 2(a) differ only by a vertical magnification, due to the difference in bead damping coefficient between model and experiment discussed in Sec. II B. We therefore now focus on the diffusion coefficients, which show significant variation among modeling and experimental results in Fig. 2(b).

As we have shown analytically [31] and graphed in Figs. 2(b) and 2(d) the diffusion coefficients for beads connected to a fixed bead attachment point by a nonlinear tether and no tether fall on a constant value and part of an inverted parabola, respectively. [In Fig. 2(d) to make these shapes visible the optical force was decreased to 0.25 pN.] These results are independent of the steric interactions and optical force, which only change the part of the line or parabola on which the coefficients fall. The direct numerical simulations of Fig. 2(d) are in excellent agreement with the analytical predictions, and Fig. 2(b) (crosses and triangles) shows that inclusion of a motor structure, in this case myosin V, does not significantly affect the shapes of these predicted curves. Thus the type of bead attachment may be discernible from the shape of the diffusion coefficient, and from this coefficient alone.

We now compare the diffusion coefficients of the two attachment types against the experimental time series. The drift and diffusion coefficients for experimental data in Fig. 2 are (statistically) stationary within each waiting period, in that the curves shown are robust to sampling smaller sections of the time series. This stationarity does not hold across intervening steps. Two of the eight waiting periods exhibit diffusion coefficients that are constant functions of position, within experimental error, while the other six are increasing. The motor-bead complex appears not to have one unique waiting conformation, but to have at least two such waiting states.

Transitions between the pre-phosphate-release and telemark states in our myosin V model do not produce changes in the diffusion coefficients matching the two shapes in Fig. 2(b), nor did we find any correlation between the shapes of these diffusion coefficients and distance from the optical trap. As discussed above, a constant diffusion coefficient is, however, consistent with the presence of an elastic tether. We can infer from the drift coefficients in Fig. 2(a) for the two time series with constant diffusion coefficients that the elasticity of this tentative tether is nonlinear (see also Ref. [31]). The other six time series exhibit diffusion coefficients that are consistent with a rigid bead attachment, as for a bead attached with no tether, or more precisely are consistent with a time scale of fluctuations in the length of the tether much shorter than the sampling interval. The different waiting states observed in the bead dynamics might therefore correspond to changes in the structure of the tether, its attachment to the bead, or possibly in optical trap alignment.

Cappello *et al*. [10] observed during waiting periods large and relatively frequent forward excursions of the bead, see for example Fig. 1(f) around 2300 μs. This forward bias is evident in the long forward tails in the experimental probability distributions of Fig. 2(c). Long forward tails are also present in the probability distributions of the myosin V model plotted in Fig. 2(c) (black lines) and the fixed-attachment-point model in Fig. S3(c) of Ref. [31]. A possible forward excursion is also visible in the sample model time series in Fig. 1(e) near 3700 μs. Therefore these excursions may be a natural feature of the bead during waiting periods rather than, as Cappello *et al*. suggested, chemical state changes associated with "aborted attempts [at] stepping." Both conclusions are consistent with current experimental data; further experiments and modeling would be necessary to distinguish them.

V. LIMITS TO RESOLVING MOTOR MOTION IN BEAD SIGNAL

We now investigate and quantify what factors can limit the ability to observe motor dynamics from bead position time series.

Brownian fluctuations of the bead can make motions of the motor to which it is connected difficult to observe. Figure 3(a) shows how the standard deviation in bead position at equilibrium, or bead noise, varies with optical force, which would not occur with a linear bead-motor connection [24]. Although in the data available to us, the bead noise of Cappello *et al*. [10] in these states did not display any such correlation, dependences of bead noise on optical trapping force similar to those in Fig. 3(a) were observed in other assays [7,22]. For a bead connected with a nonlinear tether, the increasing optical force extends the tether into a higher stiffness region, decreasing the bead noise. In the no tether case, steric interactions between the bead and motor neck

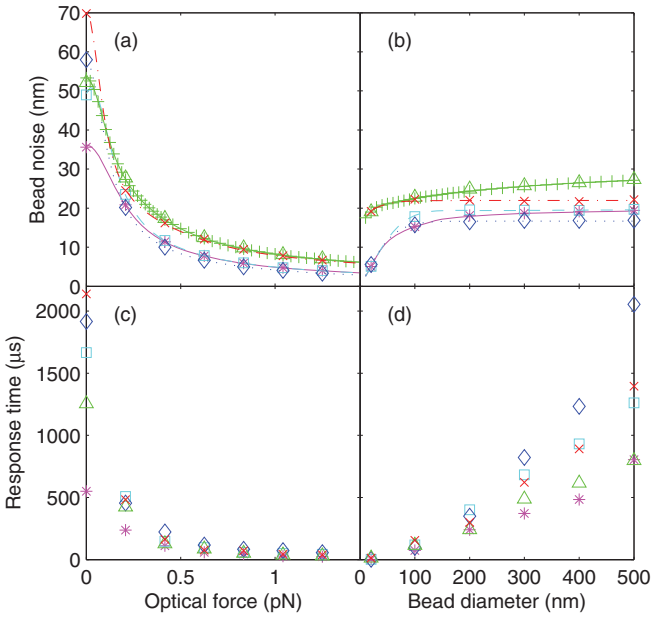

FIG. 3. (Color online) (Top) Standard deviation of the bead fluctuations, or bead noise, and (bottom) response time of the bead, according to the fixed-attachment-point model, as functions of (left) optical tweezer force with 200 nm bead diameter and (right) bead diameter with 0.25 pN optical force in the $-x$ direction. Results were calculated from direct numerical simulation of the fixed-attachment-point model (markers) and from the approximate analytical model (lines, bead noise only). The methods used to predict response times are described in Sec. III B. Line and marker colors and styles for the different bead attachments and steric interactions are as listed in Table I.

domain or substrate, or the restricted tether length, provide barriers to the bead's rotation. As the optical force increases, the bead's range of Brownian motion is compressed against the barrier, reducing the bead noise. It is remarkable that the dependence of bead noise on optical force for the different bead attachment models are so similar, considering the different physical origins of the nonlinear stiffness. At zero or very low optical force, other barriers to motion determine the bead noise.

Figure 3(b) shows that the bead noise has little dependence on the bead's size. The exception is at very small sizes, particularly for a bead attached with no tether, where the small diameter means the bead's center cannot move far. At this limit the bead noise should scale with the bead's diameter d, since this determines the range of the bead's motion.

A second mechanism limiting the resolution of motor dynamics from bead time series is the temporal response of the bead. Figures 3(c) and 3(d) plot the characteristic response time of the bead to small perturbations from equilibrium. Figure 3(c) shows that, like for the bead noise, increasing optical force rapidly decreases the response time through changes in the effective bead-motor stiffness. Nishiyama *et al.* [7] observed a qualitatively similar dependence on optical force in their kinesin bead assay.

As a function of bead diameter [plotted in Fig. 3(d)] there are two possible extremes in the response time's behavior. Where the bead motion is dominated by extensions in the tether, or constrained by optical forces to diffusion on a small region of a sphere, the response time scales with d. (Many previous authors have anticipated such a dependence on bead diameter based on Stokes' law.) Where the bead motion is dominated by diffusion on a sphere, the response time scales with d^3 [31]. At d less than about 80 nm, beads attached with no tether enter this latter regime (although this transition is less defined in the blue diamonds, no steric effects case), while the nonlinear tether models remain dominated by tether length fluctuations.

The response times of Figs. 3(c) and 3(d) are valid only for small perturbations to the bead attachment point. We also consider the response of the bead to perturbations that are not small. Figure 4 shows the response of the bead to a 36 nm step of the bead attachment point, averaged over many realizations of the process (as in Figs. 3 and 4 of Cappello *et al.* [10]). Although the motor step is instantaneous, the bead response shows two distinct phases at the optical force chosen. The "fast response" phase has the bead following the motor step almost exactly. This is more significant for a bead attached with no tether (dark blue trace with diamond, light blue trace with square, and purple trace with asterisk), where the restricted tether length combined with steric interactions means the bead cannot lag more than $d/2$ behind its attachment point. The bead in the nonlinear tether model (red trace with cross and green trace with triangle) does not have such limits to its motion, but fast and slow regions can also be distinguished due to the changing stiffness of the tether with extension. The slow response phases have the bead-motor connections relaxing on a time scale similar to that predicted in Figs. 3(c) and 3(d).

Cappello *et al.* [10] observed two similar fast and slow phases in their experiments on myosin V and ascribed them to the power stroke and diffusional search phases of the

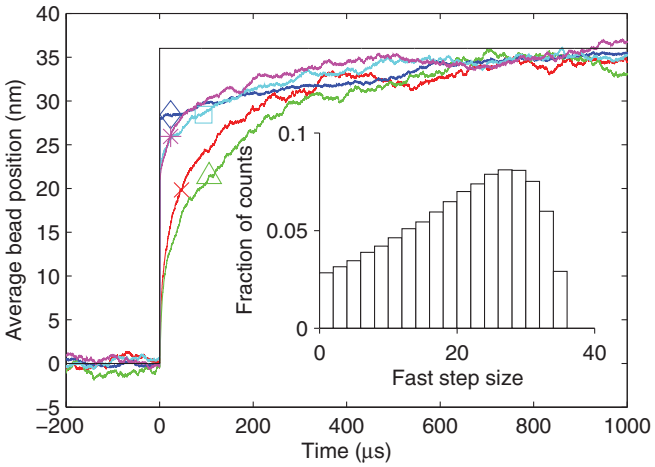

FIG. 4. (Color online) Averaged bead responses to an instantaneous 36 nm step of the motor (black line), under different bead attachment models. Line colors are as listed in Table I, with one marker as per that Table included to aid interpretation of the figure when printed in black and white. The position axis is relative to the mean position of the (averaged) bead before the step. The average was performed over 500 realizations of the step. The optical force was 0.25 pN in the $-x$ direction and the bead diameter 200 nm. Further details of the simulation are provided in Ref. [31]. (inset) A histogram of the fast phase size for a bead connected with no tether, moving in the presence of a substrate and undergoing steric interactions with the trailing motor leg (purple trace with asterisk marker in the main figure).

motor, respectively. The characteristic relaxation time of their diffusional search phase, at 1300 ± 300 μs, is substantially slower than those of the bead responses in Fig. 4, which exhibit characteristic relaxation times of around 200 μs. This difference suggests that two different motor phases are indeed present in the experiment of Cappello *et al.*, and are not in this case a result of bead dynamics alone. (If a larger model bead damping coefficient is appropriate due to surface effects, however, as discussed in Sec. II B, the longer response time may bring the bead response time closer to the characteristic time of the diffusional search phase in the experiment, possibly making the distinction between bead dynamics and motor dynamics less clear.) The presence of two motor phases is also supported by other evidence [11,16,18].

The inset in Fig. 4 shows a histogram of these fast bead phases that could be (in this simulation) falsely attributed to a fast motor substep. The variance in the size of the fast phase is very large. In fact, during many motor steps (around 15% of motor steps), the bead happened to be so far forward that it was not forced into a fast motion of any size.

The fast substep histogram shown is for a bead attached with no tether. Under this attachment, there is a maximum distance that the bead may lag behind the motor, depending on the size of the bead and the steric interactions it experiences (see Fig. S2 in Ref. [31]). The fast substep sizes were calculated as the difference between the initial bead position {determined by the distribution in Fig. S3(c) of Ref. [31]} and the position of the bead when at maximum lag behind the new motor position. Therefore no analysis of bead position time series was involved. In practice, however, measuring substep sizes

from experimental time series is a difficult task [5], and the shape of the histogram will depend on the technique used to extract the substeps and estimate their sizes. The mean value of the fast substep size is also strongly dependent on the bead size, optical force, and other experimental parameters.

VI. EFFECT OF THE BEAD ON THE MOTOR

Figure 5 plots the average time for the motor to complete a step using the myosin V model, which incorporates motor structure. The average stepping time for the motor without a bead is also shown for comparison. For the nonlinear tether attachment at zero optical force, the average stepping times are similar to that of the motor without a bead. If larger optical forces are used, for example, as discussed in the previous section to achieve small bead noise or fast response time, the bead pulls the motor further from the next binding site, making the completion of the step less likely. A slower stepping time also leads to lower processivity, that is, the motor is likely to take fewer steps before detachment.

A bead attached by no tether (blue diamonds and purple asterisks in Fig. 5) has overall more effect on the motor than one attached with a nonlinear tether (green triangles and red crosses), as measured by comparison to the stepping time without a bead. This is mostly due to steric interactions between the bead and motor. At zero optical force, the bound neck domain is on average tilted forwards; a bead attached with no tether is therefore constrained by steric interactions to be on average forward of the neck juncture (see Fig. S2 in Ref. [31]). Due to its own steric interactions with the bead, this obstructs the unbound head's search for the next binding site (see blue diamonds in Fig. 5).

A substrate, in contrast, keeps the bead attached with no tether on average further away from the binding site, and Fig. 5 (purple asterisks) shows the stepping time returns to near that for no bead. Therefore the presence of a substrate could allow one to obtain the benefits of a bead attached with no tether described elsewhere in this article, while maintaining a motor with good processivity.

An optical force of 0.1 pN is already sufficiently strong to have a bead attached by no tether located on average behind the neck juncture. Steric interactions with the backward-tilted bead cause the unbound head to preferentially search the space forward of the neck juncture. In the case of no substrate, the stepping time may be slightly faster than at zero optical force (see blue diamonds in Fig. 5). With this experimental configuration, then, there may exist an optimal nonzero optical force for high processivity.

The backward tilted bead with no tether will inevitably contact the bound neck domain. At large optical force, this distorts the bound neck domain so the neck juncture is 4–5 nm further back than without steric effects. The bound neck domain is forced to curve around the bead. This extra distance is sufficient to significantly decrease the likelihood of the unbound head finding the next binding site (compare blue diamonds and purple asterisks with red crosses and green triangles in Fig. 5).

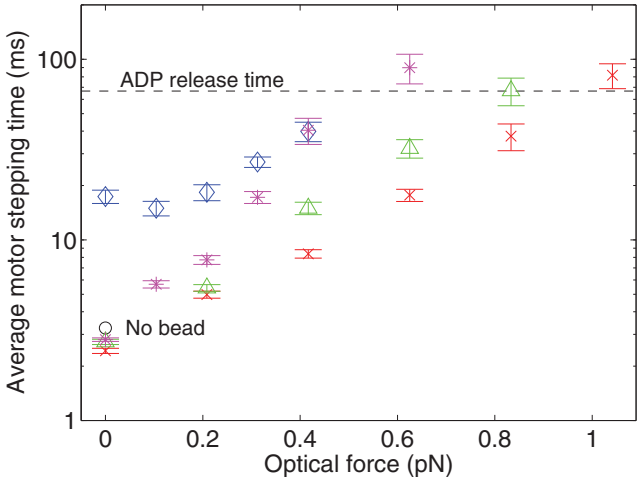

FIG. 5. (Color online) Average time for myosin V to complete a step, from detachment of trailing head until rebinding at next binding site, as a function of optical force. Marker colors and shapes are as listed in Table I. Stepping times were calculated by the method of Craig and Linke [30], where it is called "diffusion time." The calculation only considers the mechanical aspects of a step, not any chemical transitions such as ATP hydrolysis required to complete a step. The intersections of the curves with the black dashed line (the average ADP release time for the remaining bound head [30], assumed force independent) give approximate stall forces. The stepping time for a motor with no bead (and no optical force) is also shown (circle).

VII. DISCUSSION

For detecting shifts in the mean position of a motor, such as a substep, small bead noise is important. A fast response time is important for detecting dynamic behavior, such as motor stepping behavior or the presence of short-lived substeps or other intermediate states.

Both small bead noise and fast response time can be achieved with an optical force above 0.5 pN (Fig. 3), which pushes the bead-motor connection into a stiff regime for the bead attachments considered here. For the parameters used here, at such large optical forces the bead noise for the bead attached with no tether [dark blue diamonds/dotted lines, light blue squares/dashed lines, and purple asterisks/solid lines in Fig. 3(a)] is about half that for the nonlinear tether (red and green), but still reaches 30 nm. This is comparable to myosin V's step size [43] and significantly larger than the step size of kinesin [22] and the substeps of myosin V and kinesin of recent interest [7,10,16]. The latter features may be difficult to detect with these parameters, or require sophisticated data processing. At optical forces above 0.5 pN, the characteristic response time of a 200 nm bead is around 20–100 μs, except for a bead attached with no tether and with no steric effects [dark blue diamonds in Fig. 3(c), though not observable at the scale shown]. This response time is on the time scale of motor-dynamical features proposed for myosin V [10] and kinesin [4,5], indicating these features are just detectable at these parameters. (If a larger model bead damping coefficient is appropriate due to surface effects, as discussed in Sec. II B, the longer response time means these motor-dynamical features may no longer be detectable.)

The trade-off to improved resolution from larger optical forces is their effect on the motor, for example changing the motor's stepping behavior (Fig. 5). Optical force could be increased by increasing the strength of the trapping laser [44], which could hinder detection of bead position by optical methods, or by centering the optical trap farther from the motor. Force clamps [45,46] can also control the tweezer force.

Small bead noise and fast response time can also be achieved by shrinking the bead below about 100 nm diameter; most current bead assays such as that of Cappello *et al*. [10] use a 200 nm bead. Most bead assays detect bead motion through displacement of the bead's image on a quadrant photodetector [8,11], which such very small bead diameters may render impractical [7]. Alternative detection methods not affected by small bead size [36] may be an effective method of improving assay performance.

In addition to a bead attached by an elastic tether, we investigated an attachment of small or zero length. This gave rise to steric effects that may be useful to exploit in assays to probe the structure and dynamics of molecular motors. First, steric interactions between this bead and both bound and unbound neck domains of the myosin V motor affected, in a complicated way, the motor's stepping dynamics and average stepping time (see blue diamonds and purple asterisks in Fig. 5 and discussion in the previous section). The bead could also have chemical steric effects, which were not modeled here, by obstructing the binding of ATP to the motor or the release of hydrolysis products from the binding site. Third, the steric interaction of the bead with the trailing neck when under an optical force can serve to amplify, like a lever, conformational changes in the motor. In simulations of the transition into the telemark state (illustrated in Fig. S4 of [31]), the neck juncture moves only 3 nm while the bead center moves 10 nm. The trade-off is necessarily that a bead attached with no tether interferes more with the operation of the motor than a bead on the end of a long tether.

These results also demonstrate that the motion of the bead may not have a one-to-one correspondence with the motion of the point on the motor to which it is attached, which analyses of bead assays often assume. This disparity is because the bead is not fixed relative to the motor, due to rotation of the bead about its attachment point, on average, or, in the case of the nonlinear tether attachment, changes in the length of the tether. In parametrizing their mechanochemical model of myosin V from experimental data, Craig and Linke [30] assumed that the bead moved the same distance as the neck juncture during mechanochemical transitions in those experiments. The addition of the bead in this work permits evaluation of this assumption. For the nonlinear tether attachment at high force, the assumption is valid: the average positions of the bead and neck juncture in equilibrium move the same distances in transitions between the model's three mechanical states. For a bead attached with no tether and under some optical force, however, steric interactions introduced significant differences. For example, in the transition between the telemark state and the diffusional search state the average bead position moved slightly backward while the neck juncture moved forward 15–20 nm. The correspondence is also not exact for the nonlinear tether attachment under small optical force on the bead, where the tether is sufficiently unstretched that the bead may interact sterically with the motor.

Figure 5 implies that the velocity and processivity of motors with and without attached beads (at zero optical force) also are similar, provided the bead is attached by a nonlinear tether (green triangles and red crosses), or no tether with substrate (purple asterisks). More broadly, these observations support myosin V's ability in these cases to robustly transport cargo, with negligible impact on its bead- or cargo-less behavior.

Interpretation of experimental results, we have shown, must consider possible artifacts introduced by the bead, such as the step subphases shown in Fig. 4. Coarse-grained numerical models such as those used here may help identify whether a subphase is due to the motor or the bead. A bead attached with no tether may again be beneficial, due to the fast response phase of this configuration when responding to large perturbations in attachment position.

We showed evidence supporting at least two distinct "waiting" conformations of the bead-motor complex, which do not correspond to the pre-phosphate-release and telemark states as modeled here. This observation was made with the (short-time) bead diffusion coefficients from models and experimental time series. As well as its application here, drift and diffusion analysis (or Kramers-Moyal analysis) could give further insight into results of assays such as those of Dunn and Spudich [18] for myosin V, or for assays of other molecular motors. Although we would not expect our specific conclusions about myosin V to generalize to other motors, we expect that the method could be applied to other systems in the same way to draw independent conclusions about those systems.

As shown in Eq. (11) of Ref. [31], the drift coefficient under a nonlinear tether attachment is approximately equal to the nonlinear stiffness of the tether. Therefore the tether stiffness could be obtained directly from the measured drift

TABLE II. Effects of changing the properties of the bead in a bead assay.

Bead performance	Increased optical force	Increased bead size	Shorter tether[a]
Response time	Improve	Worsen	Worsen
Bead noise	Improve	No effect[b]	Improve
Impact on motor	Worsen	Worsen	Worsen
Bead position detection	Worsen or no effect	Improve or no effect	No effect

[a]For a bead attached with no tether compared with the nonlinear tether, for the parameters used in this study. A bead attached with no tether has other, possibly beneficial consequences noted in the main text.

[b]Except for increases from very small bead size, where the bead noise will worsen (increase) as bead size increases.

coefficients. Alternatively, if the tether stiffness is known this could be a test of our model and the type of bead attachment. Figure 2(a) shows that the stiffness we used is consistent with the experimental results, within experimental error. In terms of the performance characteristics we have defined, one would expect an increased stiffness to decrease bead noise and response time (as shown in Sec. 5 of Ref. [31]) and increase the effect of the bead on the motor.

In summary, a number of compromises are involved in the design of bead assays. This article considered the effects of experimental parameters including the size of the bead, the optical trapping force, and the attachment between bead and motor; we summarize the results in Table II. Decisions between these compromises ultimately depend on the objective of the assay, for example, whether to investigate the size of substeps, or their duration, or the stepping dynamics of the motor. We also made several important comparisons between our models and experimental data. Based on experimental results, we found evidence for new motor conformations during waiting periods. From numerical results, we showed that experimental observations such as multiple phases within steps and large bead excursions that were previously attributed to motor behavior may, in some cases, have been artifacts of the bead assay. Further experimental and analytical study is needed to resolve whether these observations are features of the motor or artifacts of the bead assay.

ACKNOWLEDGMENTS

We acknowledge useful discussions with Tristram Alexander, Giovanni Cappello, and Martin Zuckermann. We thank Giovanni Cappello and Paolo Pierobon for providing their experimental data. S.L. received support from the Australian Research Council's Complex Open Systems Research Network and the Sir Robert and Helen Crompton Travel Scholarship.

[1] J. Howard, *Mechanics of Motor Proteins and the Cytoskeleton* (Sinauer Associates, Sunderland, 2001).
[2] A. Yildiz, J. N. Forkey, S. A. McKinnery, T. Ha, Y. E. Goldman, and P. R. Selvin, Science **300**, 2061 (2003).
[3] A. Yildiz, M. Tomishige, R. D. Vale, and P. R. Selvin, Science **303**, 676 (2004).
[4] C. Hyeon and J. N. Onuchic, Proc. Natl. Acad. Sci. USA **104**, 17382 (2007).
[5] S. M. Block, Biophys. J. **92**, 2986 (2007).
[6] C. M. Coppin, J. T. Finer, J. A. Spudich, and R. D. Vale, Proc. Natl. Acad. Sci. USA **93**, 1913 (1996).
[7] M. Nishiyama, E. Muto, Y. Inoue, T. Yanagida, and H. Higuchi, Nat. Cell Biol. **3**, 425 (2001).
[8] N. J. Carter and R. A. Cross, Nature (London) **435**, 308 (2005).
[9] S. Verbrugge, Z. Lansky, and E. J. G. Peterman, Proc. Natl. Acad. Sci. USA **106**, 17741 (2009).
[10] G. Cappello, P. Pierobon, C. Symonds, L. Busoni, J. C. M. Gebhardt, M. Rief, and J. Prost, Proc. Natl. Acad. Sci. USA **104**, 15328 (2007).
[11] S. Uemura, H. Higuchi, A. O. Olivares, E. M. De La Cruz, and S. Ishiwata, Nat. Struct. Mol. Biol. **11**, 877 (2004).
[12] M. L. Walker, S. A. Burgess, J. R. Sellers, F. Wang, J. A. H. III, J. Trinick, and P. J. Knight, Nature (London) **405**, 804 (2000).
[13] S. Burgess, M. Walker, F. Wang, J. R. Sellers, H. D. White, P. J. Knight, and J. Trinick, J. Cell Biol. **159**, 983 (2002).
[14] E. Toprak and P. R. Selvin, Annu. Rev. Biophys. Biomol. Struct. **36**, 349 (2007).
[15] A. Vilfan, Frontiers Biosci. **14**, 2269 (2009).
[16] C. Veigel, F. Wang, M. L. Bartoo, J. R. Sellers, and J. E. Molloy, Nat. Cell Biol. **4**, 59 (2001).
[17] J. A. Spudich and R. S. Rock, Nat. Cell Biol. **4**, E10 (2002).
[18] A. R. Dunn and J. A. Spudich, Nat. Struct. Mol. Biol. **14**, 246 (2007).
[19] O. A. Oke, S. A. Burgess, E. Forgacs, P. J. Knight, T. Sakamoto, J. R. Sellers, H. White, and J. Trinick, Proc. Natl. Acad. Sci. USA **107**, 2509 (2010).
[20] K. C. Neuman and S. M. Block, Rev. Sci. Instrum. **75**, 2787 (2004).
[21] K. Svoboda and S. M. Block, Annu. Rev. Biophys. Biomol. Struct. **23**, 247 (1994).
[22] K. Svoboda, C. F. Schmidt, B. J. Schnapp, and S. M. Block, Nature (London) **365**, 721 (1993).
[23] J. Gelles, B. J. Schnapp, and M. P. Sheetz, Nature (London) **331**, 450 (1988).
[24] K. Svoboda and S. M. Block, Cell **77**, 773 (1994).
[25] J. Jaud, F. Bathe, M. Schliwa, M. Rief, and G. Woehlke, Biophys. J. **91**, 1407 (2006).
[26] M. J. Schilstra and S. R. Martin, J. R. Soc. Interface **3**, 153 (2006).
[27] R. E. L. DeVille and E. Vanden Eijnden, Biophys. J. **95**, 2681 (2008).
[28] A. Nagy, G. Piszczek, and J. R. Sellers, Biophys. J. **97**, 3123 (2009).
[29] R. Friedrich, S. Siegert, J. Peinke, S. Lück, M. Siefert, M. Lindemann, J. Raethjen, G. Deuschl, and G. Pfister, Phys. Lett. A **271**, 217 (2000).
[30] E. M. Craig and H. Linke, Proc. Natl. Acad. Sci. USA **106**, 18261 (2009).
[31] See Supplemental Material at http://link.aps.org/supplemental/10.1103/PhysRevE.84.021907 for the derivation of the fixed attachment point models; details of the extensions to the mysoin V model; derivations of scaling behaviors; and supplementary simulations exploring height-dependent diffusion coefficients.
[32] I. Schwaiger, C. Sattler, D. R. Hostetter, and M. Rief, Nat. Mater. **1**, 232 (2002).
[33] S. J. Lade, Phys. Rev. E **80**, 031137 (2009).
[34] H. Risken, *The Fokker Planck Equation: Methods of Solution and Applications*, 2nd ed. (Springer, Berlin, 1989).
[35] S. J. Lade, Phys. Lett. A **373**, 3705 (2009).
[36] L. Busoni, A. Dornier, J.-L. Viovy, J. Prost, and G. Cappello, J. Appl. Phys. **98**, 064302 (2005).
[37] F. Böttcher, J. Peinke, D. Kleinhans, R. Friedrich, P. G. Lind, and M. Haase, Phys. Rev. Lett. **97**, 090603 (2006).

[38] D. J. Evans and G. Morriss, *Statistical Mechanics of Nonequilbrium Liquids*, 2nd ed. (Cambridge University Press, Cambridge, 2008), Chap. 4.
[39] B. Lindner, New J. Phys. **9**, 136 (2007).
[40] M. Saxton, Biophys. J. **72**, 1744 (1997).
[41] P. Jung and H. Risken, Z. Phys. B **59**, 469 (1985).
[42] S. Kriso, J. Peinke, R. Friedrich, and P. Wagner, Phys. Lett. A **299**, 287 (2002).
[43] A. D. Mehta, R. S. Rock, M. Rief, J. A. Spudich, and M. S. Mooseker, Nature (London) **400**, 590 (1999).
[44] T. T. Perkins, Laser Photon. Rev. **3**, 203 (2009).
[45] W. J. Greenleaf, M. T. Woodside, E. A. Abbondanzieri, and S. M. Block, Phys. Rev. Lett. **95**, 208102 (2005).
[46] K. Visscher, M. J. Schnitzer, and S. M. Block, Nature (London) **400**, 184 (1999).